Metallurgical and Materials Transactions A 46 (2015) 665-673

Cracks in martensite plates as hydrogen traps in a bearing steel

W. Solano-Alvarez[a], Eun Ju Song[b], Do Kyeong Han[b], Dong-Woo Suh[b], H. K. D. H. Bhadeshia[a,b]

[a] *Materials Science and Metallurgy, University of Cambridge, U.K*

[b] *Graduate Institute of Ferrous Technology, POSTECH, Republic of Korea*

Abstract

It is demonstrated that a macroscopically homogeneous distribution of tiny cracks introduced into a martensitic bearing steel sample can provide powerful hydrogen traps. The phenomenon has been investigated through thermal desorption spectroscopy and hydrogen permeation measurements using both cracked and integral samples. The effective hydrogen diffusion coefficient through the cracked sample is found to be far less than in the uncracked one. Similarly, when samples are charged with hydrogen, and then subjected to thermal desorption analysis, the amount of hydrogen liberated from the cracked sample is smaller due to the trapping by the cracks. Theoretical analysis of the data shows that the traps due to cracks are so strong, that any hydrogen within the cracks can never in practice de-trap and cause harm by mechanisms that require the hydrogen to be mobile for the onset of embrittlement.

Keywords: hydrogen trapping, thermal desorption spectroscopy, microcracks, bearing steel 52100, hydrogen permeation

1. Introduction

The vast majority of bearing steels are manufactured to be extremely hard in order to resist rolling-contact stresses of the order of 2 GPa. The steels typically contain 1 wt% of carbon and 1.5 wt% Cr so that they can be

processed into a martensitic microstructure, which is then subjected to a low-temperature tempering heat-treatment that has the dual purpose of reducing the retained austenite content to a level consistent with dimensional stability requirements, and to improve the properties of the martensite [1].

Like most strong steels, the ingress of hydrogen leads to a severe degradation of the mechanical properties of bearing steels, even at concentrations as small as 1 part per million [2, 3]. In the case of bearings, hydrogen can cause premature failure at 1-10% of the expected life (L_{10}) through embrittlement that is revealed in the microstructure as white-etching regions [2, 4]. This "white-etching matter" is seen as a form of damage whereby repeated deformation mechanically homogenises the structure and reduces its length scale to the nanometre range. The subject has been reviewed extensively but it is well known that hydrogen exacerbates the problem [1, 4]. The hydrogen that enters the steel can be generated by the decomposition of lubricants, through corrosion reactions, or exposure to hydrogen sources; this is why even 10 ppmw of water dissolved in lubricant can be harmful [5–8].

Given the low overall concentration of hydrogen that embrittles steel, many of the mechanisms that explain the effect require the accumulation of hydrogen by diffusion towards regions of the steel where the stress is focussed [9, 10]. The resulting increase in hydrogen concentration there leads, for example, to localised plastic instability and failure[1]. Therefore, it is diffusible (monoatomic) hydrogen that causes harm. That which is strongly trapped or present in molecular form can be considered in most cases to have been rendered harmless [13, 14]. Traps can be varied, for example those which attract hydrogen through stress fields (grain boundaries, inclusions, dislocations, crack tips, carbides) [15] or others where hydrogen simply accumulates through random encounters (voids, retained austenite).

We recently have developed methods of introducing microscopic cracks into bearing steel [16, 17]; the original aim was to investigate white-etching matter generation when the cracked samples are subjected to rolling contact stresses. In hindsight, the improvement in rolling contact fatigue experienced

[1]There are alternative interpretations: hydrogen-enhanced decohesion [11] although it has been shown using first principles calculations that this may not be potent [12], but it is noteworthy that this also requires the diffusion of hydrogen to maintain crack propagation [9].

for cracked samples might have been expected because bearing steels are comparatively brittle, and microscopic cracks help to deflect fatigue damage, a well-known phenomenon in artificial composites. It was felt that it would be interesting to examine the role of the microscopic cracks as traps for hydrogen. The corollary is that the work might be applicable to inclusions that have weak interfaces with the steel matrix, that also should act in a manner similar to the cracks in accumulating hydrogen and keeping it there in molecular form.

2. Experimental Methods

2.1. Material

The hot-rolled and spheroidised 52100 steel used (table 1), was cut using an electrical discharge machine into thin rectangular samples 40 mm long, 12 mm wide, and 2 mm thick for the hydrogen thermal desorption spectroscopy tests and into thin squares 20 mm a side and 2 mm thick for measuring hydrogen permeation.

Table 1: Chemical composition, wt%, of the 52100 steel used.

C	Cr	Mn	Mo	Si	Ni	Al	P	S	Cu	Co	Ca	Ti
0.98	1.38	0.28	0.06	0.28	0.18	0.04	0.01	0.017	0.21	0.015	0.001	<0.001

2.2. Heat treatments

Two different processes were applied to the samples, the standard heat treatment for 52100 steel and the extensive martensite-plate cracking treatment described in [16]. The former consists of austenitisation at 1113 K (840 °C) for 20 min followed by quenching in oil at room temperature and then tempering at 433 K (160 °C) for 2 h. Some of the cementite does not dissolve during this austenitisation treatment, so spheroidal (up to 2 μm in diameter), proeutectoid particles are inherited in the final structure that also contains much finer carbides resulting from the tempering of martensite.

To produce samples in which the martensite plates are microscopically cracked, samples were austenitised at 1313 K (1040 °C) for 30 min, cooled in

air for 50 s, quenched in oil at room temperature, and tempered at 433 K (160 °C) for 2 h [16]. The higher austenitisation temperature dissolves all the cementite so the only carbides that are in the microstructure are those resulting from the tempering treatment [18].

2.3. Specimen preparation

After heat treatment, the thermal desorption samples were ground with 800 grit sandpaper to achieve the required finish, whilst the permeation samples were ground down to ∼0.5 mm in thickness using a Struers AbraPlan-20 automatic rock grinding machine and then manually ground with 1200 grit sandpaper for the desired surface roughness. A few samples were then prepared for metallographic examination using a Zeiss optical microscope to confirm the desired microstructure and a good density of cracks were formed.

2.4. Thermal Desorption Spectroscopy (TDS)

Due to the difference in heat treatments, the integral (crack-free) and cracked specimens have different grain sizes, carbide volume fraction, and in particular retained austenite, which might make the study of the role of cracks as trapping sites uncertain. Since the binding energy of cementite is smaller than that of dislocations or grain boundaries and is approximately an order of magnitude lower than that cracks [19–21], the focus of the experiment design was to separate the role of retained austenite content due to the large difference in hydrogen diffusivity between ferrite and austenite.

Three different thermal desorption experiments were designed:

1. **Partially charged samples:** 7 h hydrogen charging, desorption measurement during ramped heating at 100 K h^{-1} (100 °C h^{-1}) until 673 K (400 °C), hydrogen recharging for other 7 h and a second ramped heating desorption measurement at the same heating rate to compare the influence of cracks after retained austenite decomposition.
2. **Isothermal experiments:** 7 h hydrogen charging and desorption measurement during isothermal heat-treatment at 363 K (90 °C) for 4 h as an alternative method to evaluate hydrogen trapping by cracks.
3. **Prolonged charging experiments:** 120 h hydrogen charging and desorption measurement during ramped heating at 100 K h^{-1} (100 °C h^{-1})

until 673 K (400 °C) (no recharging) to study a greater level of saturation in the samples, which would tend to reduce the significance of traps in thermal desorption experiments as hydrogen diffusing through the sample would not be attracted into saturated traps. This condition can provide a better indication of the consequences of local equilibrium between ferrite and austenite.

The seven hour charging time is to ensure that samples are not saturated meaning that the hydrogen concentration in spatially non-uniform due to the diffusion front not reaching the centre of the sample, so if strong traps exist, the amount of hydrogen released during thermal desorption would be limited when compared with a sample without the cracks. The temperature readings of the furnaces were calibrated with the actual specimen temperature by welding a thermocouple to each sample.

Initially, all of the samples were electrochemically charged with hydrogen using a 3% NaCl + 0.3% NH_4SCN solution and a current density of $1\,A\,m^{-2}$. The charging current was calculated by considering only the area of the top and bottom surfaces of the samples and not the sides, given their low thickness. For samples with ramped heating, TDS testing started 45 min after charging and for the isothermal desorption, only 20 min after in order to allow the readily diffusible hydrogen to leave the sample and for the TDS machine to purge out the air introduced in the system when the sample is placed in the tube furnace. Using an Agilent Technologies 7890A gas chromatography system coupled to an EPKRO-12K Isuzu tubular furnace and a Seahwa SERO2000-1CH flow regulator, hydrogen desorption data were collected every 3 min from which the hydrogen content was calculated as the area under the curve divided by the heating rate, and the desorption rate as the evolved hydrogen per minute. Helium was used as the carrier gas and a standard mixture of He + 60 ppmv H_2 was used for calibration.

2.5. Retained austenite

In order to investigate the volume fraction of retained austenite before and after TDS heating to 673 K (400 °C), XRD spectra were obtained using a Philips PW1830 vertical diffractometer with a CuK_α radiation. Scans were performed from 40 to 125 °, with a step size of 0.05 ° and a dwell time of 26 s. A divergence slit of 0.5 °, an anti-scatter slit of 0.5 °, and a receiving slit of

0.2 mm were used to restrict the beam size and the counts obtained. The volume fractions of martensite and austenite were obtained using High Score plus and the Rietveld refinement method by fitting body-centred tetragonal martensite to two isolated martensite peaks (020 and 121) for each spectrum. This pair of values of tetragonality were then used as minimum and maximum limits in the fitting of lattice parameters for martensite to the whole spectrum. This process is described in more detail in [17].

The onset of retained austenite decomposition was investigated prior to TDS analysis by heating up separate un-cracked and cracked samples in a Theta Industries Dilatronic III using a heating rate of $100\,\mathrm{K\,h^{-1}}$ ($100\,^{\circ}\mathrm{C\,h^{-1}}$) up to 723 K (450 °C) and quenching at $50\,\mathrm{K\,s^{-1}}$ ($50\,^{\circ}\mathrm{C\,s^{-1}}$).

2.6. Electrochemical Hydrogen Permeation

Using a Devanathan and Stachurski cell, hydrogen permeation tests at room temperature were conducted according to ISO 17081-2004 standard [22, 23]. After cleaning the samples in hydrochloric acid, a Pd film was deposited electrochemically by submerging one side of the sample in a solution of 2.54 g of $PdCl_2$ in 500 ml of 28% aqueous ammonia and applying for 2 min a current density of $2.83\,\mathrm{mA\,cm^{-2}}$. This coating is performed to increase the efficiency of the hydrogen oxidation reaction at the hydrogen detection side. The detection side was then filled with a 0.1 M NaOH solution at a constant potential of 250 mV. Once a a steady state current below $3\,\mu\mathrm{A\,cm^{-2}}$ was reached, the hydrogen charging side of the cell was filled with a 3% NaCl + 0.3% NH_4SCN solution and a density current of $1.5\,\mathrm{mA\,cm^{-2}}$ was applied. The hydrogen oxidation current was measured as a function of time and the effective diffusivity, permeability, and apparent solubility were calculated as described in [24].

3. Results and discussion

3.1. Basic characterisation

Optical microscopy after the heat treatment for the cracked samples confirmed the expected distribution of martensite-plate cracks [16], as shown in fig. 1a.

The XRD spectra of the cracked and un-cracked specimens before and after 120 h charging and TDS testing up to 673 K (400 °C) are presented in fig. 1b. The difference in austenitisation temperatures led to corresponding differences in the retained austenite content of 0.05±0.01 for the integral (no cracks) sample and 0.12±0.01 for the cracked one. However, the retained austenite in both samples decomposed on heating to 673 K (400 °C) during TDS. This was confirmed using dilatometry (fig. 1c). For both samples, the onset of retained austenite decomposition is at ∼548 K (275 °C).

The hardness values of the samples before and after TDS testing are presented in table 2.

Table 2: Vickers hardness for the cracked and un-cracked samples used in each of the three TDS experiments. The average value and standard error were calculated based on ten indentations per sample.

Experiment	Partially charged		Isothermal heating		Prolonged charging	
	No cracks	With cracks	No cracks	With cracks	No cracks	With cracks
Before run 1	737±3 HV30	751±4 HV30	785±2 HV30	754±3 HV30	758±2 HV30	780±1 HV30
After run 1	495±3 HV20	490±5 HV20	785±1 HV30	754±2 HV30	505±1 HV20	546±3 HV30
After run 2	493±1 HV20	489±3 HV20	-	-	-	-

3.2. Thermal Desorption Spectroscopy (TDS)

The desorption curves for each of the three TDS experiments on partially charged samples are presented in fig. 2, together with an indication of the total amount of hydrogen desorbed.

Focusing first on the cracked sample, two desorption peaks were observed, the one beyond 523 K (250 ℃) being attributed to hydrogen released when retained austenite decomposes is consistent with the dilatometric and X-ray data, and with the fact that the higher-temperature peak disappears when the sample already subjected to TDS up to 673 K (400 ℃) is recharged with hydrogen and once again studied using thermal desorption spectroscopy. Furthermore, the second peak is only perceptible in the cracked sample that has a much larger retained austenite content. It is also worth noting that the hardness of the sample does not change at all within the limits of scatter, when subjected to the second TDS experiment (table 2).

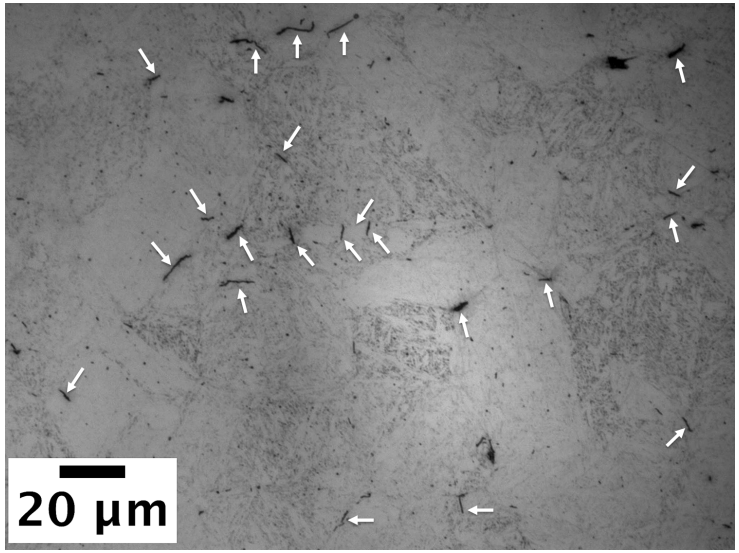

(a)

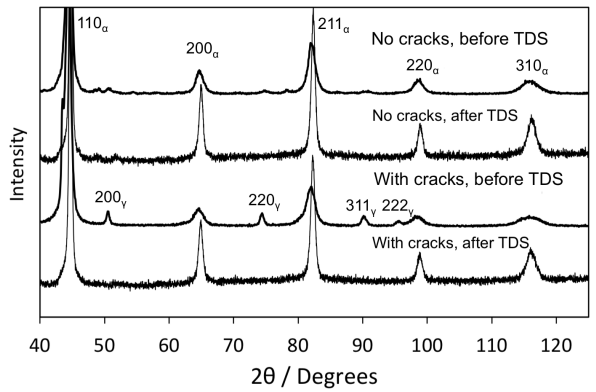

(b)

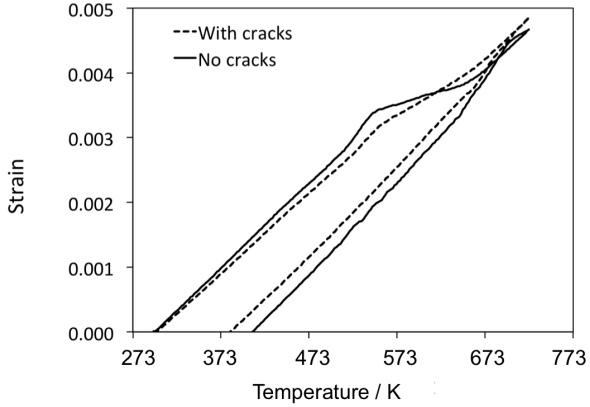

(c)

Figure 1: (a) Optical metallography of cracked sample prior to TDS testing. (b) X-ray diffraction data for retained austenite determination. (c) Dilatation curve for the cracked and un-cracked samples using the same heating rate as the first TDS experiment, $100\,\mathrm{K\,h^{-1}}$ ($100\,^{\circ}\mathrm{C\,h^{-1}}$).

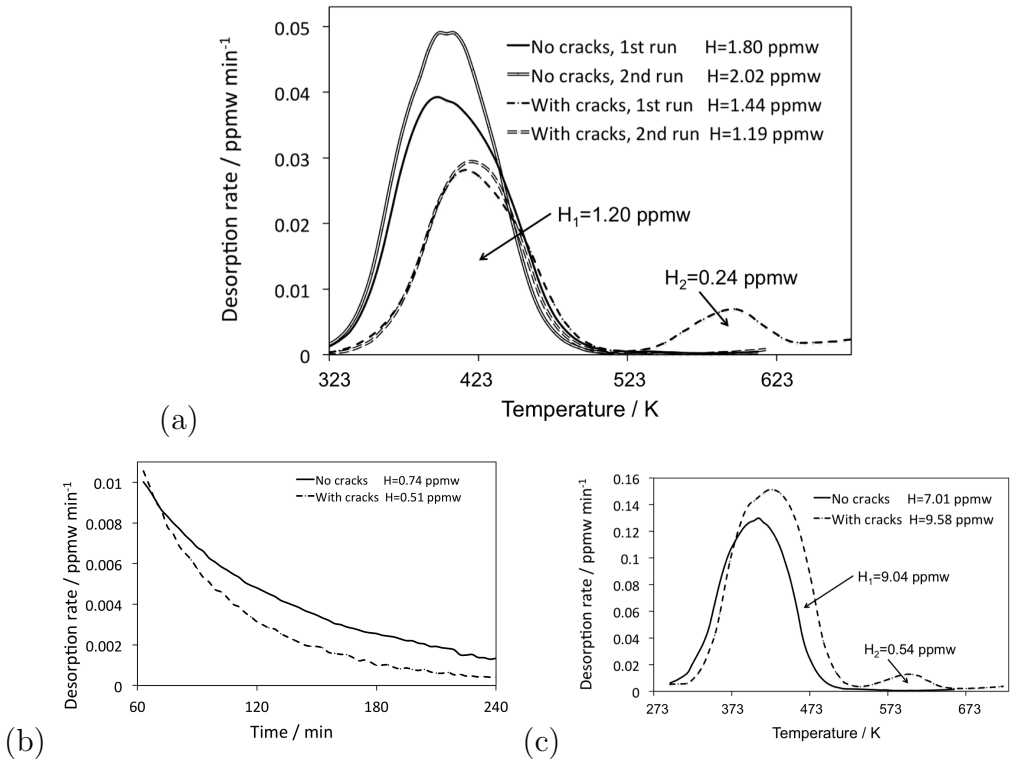

Figure 2: a) Experiment 1: Desorption during ramped heating at $100\,\mathrm{K\,h^{-1}}$ ($100\,^{\circ}\mathrm{C\,h^{-1}}$) after 7 h charging (recharged once), b) Experiment 2: Isothermal desorption at 363 K (90 °C) for 4 h after 7 h hydrogen charging (no recharging), c) Experiment 3: Desorption during ramped heating at $100\,\mathrm{K\,h^{-1}}$ ($100\,^{\circ}\mathrm{C\,h^{-1}}$) after 120 h charging, (no recharging).

It is noteworthy the un-cracked samples release more hydrogen during TDS than those containing cracks (fig. 2a), consistent with the hypothesis that in the latter case, some of the charged hydrogen will become strongly trapped. For the same reason, there is less readily diffusible hydrogen evolved below 423 K (150 ℃) from the cracked sample, resulting is a smaller TDS peak that is in effect shifted to a greater temperature. Retained austenite is not responsible for the relatively small TDS peak of the cracked sample in the temperature range below 523 K (250 ℃) because that peak does not change when the austenite is absent in the *recharged* sample.

The isothermal experiments performed at 363 K (90 ℃) and illustrated in fig. 2b confirm the interpretations above. The evolved hydrogen is about 31% less for the cracked sample.

The data for the samples that underwent prolonged charging for 120 h are particularly revealing about the role of austenite (fig. 2c). The general features of the TDS curves are similar to those of samples that were charged for only 7 h, with the cracked sample exhibiting the second desorption peak associated with the decomposition of austenite. However, there are detailed differences that arise from the fact that austenite and ferrite are in local equilibrium prior to the decomposition of austenite. The concentrations ($c = x/V$) associated with the first and second peaks, where x is the amount of hydrogen evolved over the temperature range of each peak, and V is the fraction of the phase with which that peak is associated are listed in table 3. When austenite is in equilibrium with ferrite, it has a much greater solubility for hydrogen; that is well known. However, during the desorption of hydrogen as the sample is heated, hydrogen in the ferrite escapes into the surrounding environment, and the austenite acts as a source for more hydrogen since equilibrium is maintained at the α/γ interface. This process does not require the decomposition of that austenite so the hydrogen released in the second peak beyond 523 K (250 ℃) is simply a reflection of the *remaining* quantity in the γ just before its decomposition. This explains several observations:

(a) A second peak is not observed in the sample with $V_\gamma = 0.05$ (un-cracked) because the austenite is essentially exhausted by the time the temperature reaches 523 K (250 ℃).

(b) Considering the samples that were charged for 120 h, contrary to expectations of a greater solubility in γ, the concentration $c_\gamma \ll c_\alpha$, because

the austenite releases hydrogen into the ferrite during heating as the concentration in the latter phase decreases by escape into the environment.

(c) The concentration c_α in the samples charged for 120 h is greater in the cracked than un-cracked samples. This is because the cracked sample has a reservoir of hydrogen in the 0.12 volume fraction of retained austenite, that released hydrogen into the surrounding ferrite during heating.

(d) The actual amount of hydrogen in austenite of the 120 h specimen immediately after charging and before heating, must have been much larger than indicated by the second peak (c_γ). The lower limit of this concentration, c_γ^0 can be estimated by comparing the two curves below 523 K (250 ℃) in fig. 2c. The two samples have a difference in retained austenite fraction of $0.12 - 0.05 = 0.07$, and the difference in the hydrogen released is $9.04 - 7.01 = 2.03$ ppmw. If this difference is purely due to the hydrogen released by austenite into ferrite during heating, then the total concentration is given by $c_\gamma^0 = (2.03/0.07) + (0.54/0.12) = 33.5$ ppmw. This is a much larger concentration than the c_α values listed in table 3, as might be expected from the relative solubilities of hydrogen in austenite and ferrite.

Table 3: Concentrations associated with the TDS experiments as described in the text. The accuracy of determining x_α and x_γ is approximately 0.01 ppmw [25]. The uncertainty of V_γ is 0.01 as described in section 3.1.

	V_γ	x_γ / ppmw	x_α / ppmw	c_γ / ppmw	c_α / ppmw
Cracked, partially charged	0.12	0.24	1.20	2.00±0.03	1.34±0.02
Cracked, prolonged charging	0.12	0.54	9.04	4.50±0.06	10.27±0.11
Un-cracked, partially charged	0.05	0	1.8	0±0.01	1.90±0.03
Un-cracked, prolonged charging	0.05	0	7.01	0±0.01	7.37±0.08

3.3. Hydrogen Permeation

We were not able, for practical reasons, to implement sufficient experiments to obtain conclusive results that separate out the effects of retained austenite and cracks. Both of these factors would reduce the effective diffusivity of hydrogen because the diffusivity in austenite is much smaller than

in ferrite, and cracks are such strong traps that they would also hinder the passage of hydrogen through the steel. An ameliorating factor is that the retained austenite in both samples is not in the form of films that percolate through the microstructure [26], but mostly present as blocks about 3 µm in size. Consistent with [26], such austenite would not form continuous barriers to the path of hydrogen, so it might be speculated that the role of the austenite can be neglected.

The hydrogen permeation curves for each of the two samples are presented in fig. 3. Using these data as well as the sample thickness L, the break-through time t_b, and steady-state current density I_{ss}, the values of the effective hydrogen diffusivity D_{eff}, permeation P, and apparent hydrogen solubility C_{app} were calculated using the break-through method in reference to the ISO17081 standard (table 4). Both the effective diffusivity and permeability values are much greater in the case of the un-cracked samples, potentially suggesting the role of the cracks in trapping the hydrogen as it attempts to pass through the steel.

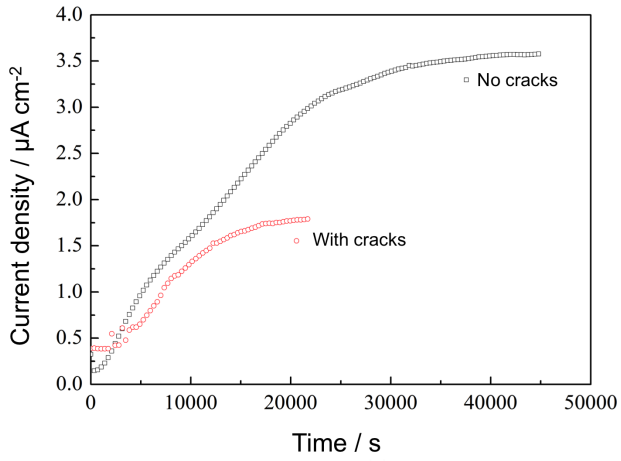

Figure 3: Hydrogen permeation curves for cracked and un-cracked samples.

3.4. Model

The purpose of the work presented here was to study primarily the influence of cracks on the thermal desorption curves in order to gain more confidence in the interpretation of experimental data. The effect of hydrogen

Table 4: Parameters determined through the hydrogen permeation test. The uncertainty of the sample thickness is ±2% and that of the diffusivity, permeation, and solubility is ±4%.

Parameters	No cracks	With cracks
L / m	0.00058	0.00062
t_b / s	420	1600
I_{ss} / $\mathrm{A\,m^{-2}}$	0.0358	0.0179
D_{eff} / $\mathrm{m^2\,s^{-1}}$	5.235×10^{-11}	1.57×10^{-11}
P / $\mathrm{mol\,m^{-1}\,s^{-1}}$	2.15×10^{-10}	1.15×10^{-10}
C_{app} / $\mathrm{mol\,m^{-3}}$	4.11	7.32

trapping at cracks during TDS experiments was simulated by adapting one of the hydrogen desorption models developed by Song et al. to include a fine dispersion of microcracks in a ferritic matrix, These cracks were modelled as surface disconnections within the matrix making them behave in a similar way to voids [27]. A key aspect of this model is that it permits multiple traps to be included in the analysis whereas none of the existing analytical methods can deal with more than one type of trap. As will be seen, a certain amount of calibration is needed to assign trap number-densities, and this was done on the basis of data collected for the samples without cracks.

In the model, the consequence of the initial charging stage is to distribute the hydrogen across the lattice and trapping sites assuming local equilibrium. The diffusion is assumed to be parallel to the thickness direction, while the hydrogen interacts with multiple kinds of traps of different binding energies: grain boundaries, dislocations, and microcracks. A more detailed explanation of the theory behind the numerical model and the consequences of different dislocation densities in hydrogen trapping can be found in [27].

The binding energies and densities of trapping sites by interfaces and dislocations were obtained from the previous study by Song et al. [27]. The reported binding energies were 49 and 44 $\mathrm{kJ\,mol^{-1}}$ for grain boundaries and dislocations, respectively. However, in those experiments the sample temperature was assumed to be that of the furnace rather than measuring the sample temperature directly, which was ∼20-30 °C higher in the 100-200 °C range. Therefore, the temperature calibration described in section 2.4 was used to correct these values to 50 and 47 $\mathrm{kJ\,mol^{-1}}$ respectively, with an uncer-

tainty of $\pm 2\,\mathrm{kJ\,mol^{-1}}$. The density N_t^ρ of trapping sites due to dislocations was calculated using equation 15 in [27]:

$$N_t^\rho = 12\pi b^2 \rho/\Omega \tag{1}$$

where b is the magnitude of the Burgers vector, $\rho = 10^{13}\,\mathrm{m^{-2}}$ is the dislocation density equal for both cracked and integral samples [28], Ω is the atomic volume of iron, yielding $N_t^\rho = 6.73 \times 10^{23}\,\mathrm{m^{-3}}$. The density of trapping sites due to interfaces, $N_t^{gb} = 1.65 \times 10^{25}\,\mathrm{m^{-3}}$, was obtained by fitting the numerical model to the TDS curves for the recharged un-cracked samples that did not contain any retained austenite but maintained their hardness after the first TDS run. It is worth mentioning that the value of diffusivity used in the model is not the one derived from the hydrogen permeation tests, affected by defects such as cracks and retained austenite, but the standard value of hydrogen diffusing through a ferritic lattice [29].

The crack number-density N_V^c=$4.1\times10^{14}\,\mathrm{m^{-3}}$ was obtained by measuring 700 cracks using metallography and assuming that the crack depth was equal to the average length. The trapping site density on the crack faces was calculated as the number of iron atoms on each of the two faces of the cracks present, per unit volume of steel. This assumed circular martensite discs of mean linear intercept $\overline{L} = 45\,\mu\mathrm{m}$ [16] and $2.25\,\mu\mathrm{m}$ in thickness (c/a aspect ratio of 0.05 [30]) knowing that there is an equivalent of 1/2 iron atom at the face of the BCC lattice. By fitting the data to the simulated curves it was possible to determine the amount of hydrogen atoms that get trapped per iron atom of the cracked surfaces.

This model allowed the simulation of the desorption of hydrogen from various kinds of traps in a purely ferritic matrix, limiting the analysis to the TDS curves of the un-cracked and cracked samples, after partially charging with hydrogen for the second time, which contained virtually no retained austenite. The closest fit to the data under the assumptions of unidirectional hydrogen flow, local equilibrium, and the three kinds of traps used (not considering trapping at cementite) is presented in fig. 4a.

By modelling the peak of the recharged cracked and integral samples in the partially charged experiment it was found that the closest fit to the data was achieved for a crack binding energy of above $200\,\mathrm{kJ\,mol^{-1}}$ assuming one hydrogen ion gets trapped by each iron atom. In fact, increasing the value up to $500\,\mathrm{kJ\,mol^{-1}}$ made no changes in the height or shape of the peak since

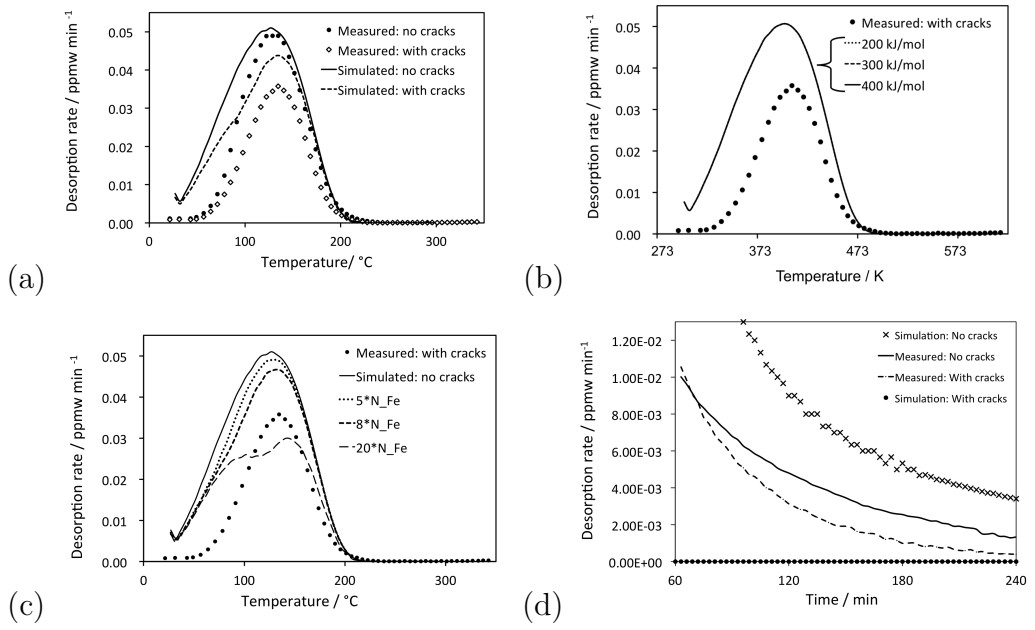

Figure 4: a) Comparison between experimental and simulated hydrogen desorption curves for cracked and integral samples (second run, partial charging), b) variation of the binding energy to fit the peak of the cracked sample after partial recharging, whilst having a constant trap density of N_{Fe}^{c}=5.1×10^{23} m^{-3} (one hydrogen ion per iron atom), c) variation of the trapping site density of cracks as a multiple of the number of iron atoms at the surface of cracks present in unit volume of steel, N_{Fe}^{c}, and d) comparison between experimental and simulated hydrogen desorption curves for cracked and integral samples containing retained austenite during isothermal heating.

all these values represent already irreversible trapping sites (fig. 4b). Since it was considered in this model that hydrogen absorbed by cracks becomes molecular inside them, the binding energy is linked to the bond dissociation energy of hydrogen, $458\,\mathrm{kJ\,mol^{-1}}$ [31], and not to that of free surfaces, 70-$95\,\mathrm{kJ\,mol^{-1}}$ [32].

By taking a binding energy above $200\,\mathrm{kJ\,mol^{-1}}$, the trapping site density of cracks was then varied to find the best fit at $N_t^c{=}41{\times}10^{23}\,\mathrm{m^{-3}}$, which is approximately eight times the amount of iron atoms calculated to be at the surfaces of cracks present per unit volume of steel ($N_{Fe}^c{=}5.1{\times}10^{23}\,\mathrm{m^{-3}}$). In other words, approximately eight hydrogen ions are actually trapped at each iron atom found at the crack surfaces, meaning that there are at least $\sim 9.95 \times 10^9$ trapping sites per crack. It is expected that once the hydrogen ions get trapped at the crack surfaces, hydrogen combines to form molecular hydrogen which fills up the volume of the crack. This means that although hydrogen adapts its molecular state which is not pernicious, desorption of it would require complete meltdown of the sample [1]. Trapping of hydrogen by cracks will saturate when the volume of the crack has been filled by molecular hydrogen which could potentially create a internal pressure that would promote crack propagation. However, this internal pressure could be beneficial in avoiding the crack surfaces to rub against each other under rolling contact fatigue, which has been suggested to be the cause to "white-etching matter" formation [17]. In other words, the presence of cracks in the bulk would not only render pernicious hydrogen immobile and not damaging, but could also limit it from fostering microstructural degradation in the form of white-etching matter.

As shown in fig. 4c, increasing the trapping site density of cracks as a multiple of N_{Fe}^c decreases the height of the peak up to a maximum of $\sim 8N_{Fe}^c$ after which the peak splits in two due to incomplete saturation at the middle of the sample that alters the diffusion distance of hydrogen. This is shown in fig. 5 where the hydrogen profile after charging, room temperature aging, and heating are plotted for the case of $N_t^c{=}8N_{Fe}^c$ and $20N_{Fe}^c$. In fig. 5d, 5e and 5f, it can be seen that in the case of the partially charged samples, hydrogen diffuses not only out through the surface, but also towards the middle of the sample after charging and before heating. Despite hydrogen diffusing inwards, the centre of the sample still remains unsaturated. After heating, there is hydrogen in the centre (fig. 5f), unlike the previous graph (fig. 5e),

trapped at cracks due to their strong binding energy. Since the depth of penetration of trapped hydrogen increased, the effective diffusion distance is longer than the sample thickness for the hydrogen that diffused into the sample after charging causing the desorption peak to split.

In an attempt to model the results of the partially charged samples containing retained austenite of the isothermal heating experiment (fig. 4d), it was found that in the un-cracked case, the simulation over-predicted the amount of hydrogen desorbed although the trend of desorption was accurate. This is due to the difference in absorbed hydrogen and effective diffusivity, knowing that the model only accounts for ferrite. However, the important part to note is that for both experimental observations and simulations, cracks have the ability to re-trap hydrogen freed from reversible traps. In the case of the cracked sample, there was no desorption since the cracks were partially charged (unsaturated) from the beginning and in fact kept trapping the hydrogen freed from low binding energy traps at 363 K (90 °C). Desorption would only occur until all the cracks are saturated. The measured cracked sample does show hydrogen desorption since the real distribution of cracks is less homogenous than the one assumed in the model so it is unlikely freed hydrogen will always meet a crack, and be re-trapped, as it effuses out.

4. Conclusions

The following conclusions can be reached from the present work, based on critical experiments using thermal desorption spectroscopy and electrochemical hydrogen permeation of 52100 bearing steel samples heat treated according to the standard procedure and through a process to develop microcracks, as well as on model developed to describe and predict the results obtained:

- Martensite plate cracks or microcracks act as irreversible traps for diffusible hydrogen in 52100 steel. When absorbed by cracks, hydrogen ions will become molecular and lose their damaging character. If not saturated, these cracks can also retrap hydrogen freed from reversible, low-binding energy traps such as dislocations or grain boundaries.

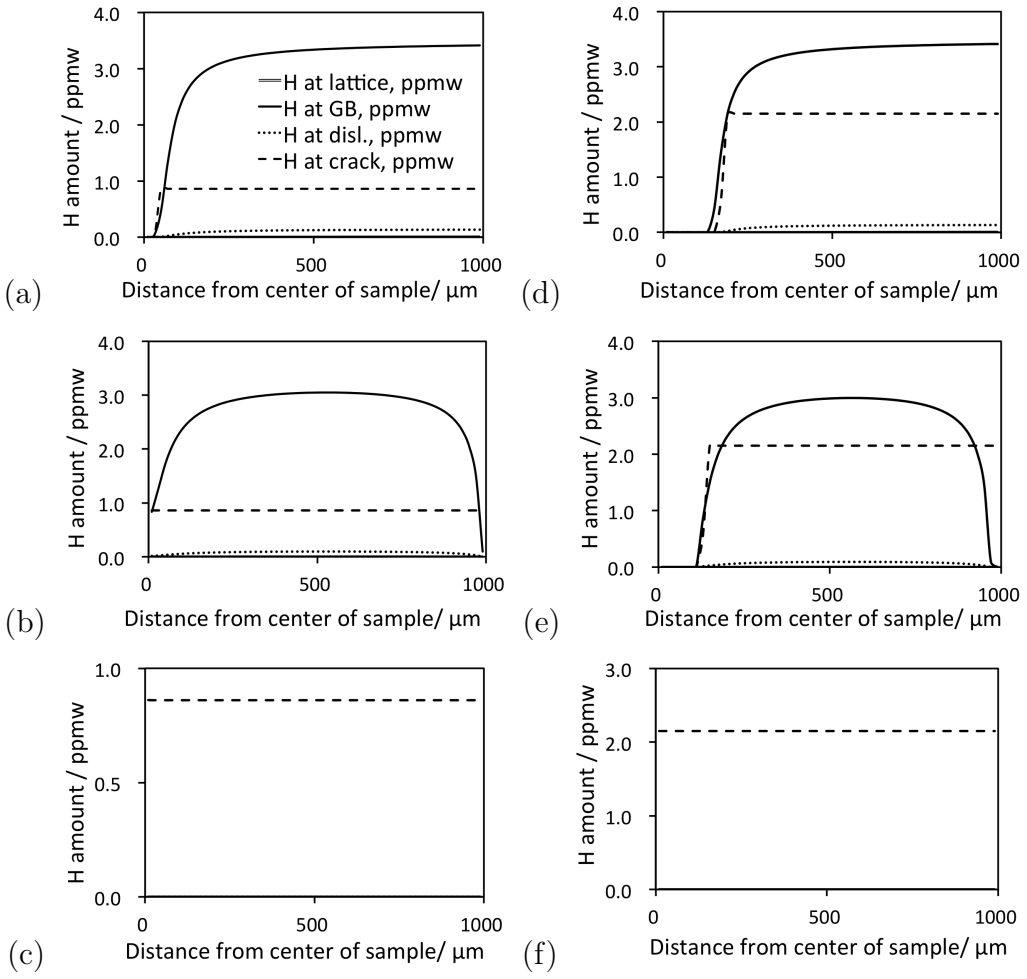

Figure 5: Hydrogen profiles in the modelled sample for $8N_{Fe}^{c}$ in the left column and $20N_{Fe}^{c}$ in the right column, where a) and d) represent the hydrogen present after charging, b) and e) the hydrogen after room temperature ageing, and c) and f) the hydrogen after heating trapped at lattice, grain boundaries (GB), dislocations, and cracks. The x-axis represents the centre of the sample (0 µm) and the surface (1000 µm), showing in d) and e) how an increased trap density leaves the centre of the specimen uncharged.

- As confirmed by XRD and dilatometry, partially charged and supersaturated hydrogen samples containing around 0.12 volume fraction of retained austenite showed a second peak in ramped heating TDS experiments corresponding to the hydrogen desorption caused by retained austenite decomposition at $\sim$548 K (275 °C). The samples heat treated according to the standard procedure containing around 0.5 volume fraction of austenite after tempering did not show such second peak.

- Through electrochemical permeation tests, the effective hydrogen diffusivity D_{eff} was found to be $5.235 \times 10^{-11}\,m^2\,s^{-1}$ for the crack-free sample and $1.57 \times 10^{-11}\,m^2\,s^{-1}$ for the cracked sample. The experiment also allowed to obtain the apparent hydrogen solubility C_{app} which is $4.11\,mol\,m^{-3}$ for the crack-free sample and $7.32\,mol\,m^{-3}$ for the one with cracks.

- A model assuming local equilibrium was able to reproduce the hydrogen desorption behaviour of the integral (crack-free) and cracked samples containing no retained austenite by taking into consideration the effect of multiple binding energy traps such as grain boundaries, dislocations, and cracks.

- The binding energy for cracks was estimated to be of at least $200\,kJ\,mol^{-1}$, whereas the density of cracks was measured to be N_V^c=$4.1\times10^{14}\,m^{-3}$, and the trapping site density generated by cracks N_t^c=$41\times10^{23}\,m^{-3}$.

5. Acknowledgements

The authors are thankful to other members of the Computational Metallurgy Laboratory at GIFT and from the Phase Transformations and Complex Properties Group at Cambridge University. W. Solano-Alvarez is very grateful for support from the Worshipful Company of Ironmongers, CONACyT, the Cambridge Overseas Trust, and the Roberto Rocca Education Programme.

6. References

[1] H. K. D. H. Bhadeshia: Progress in Materials Science 2012, vol. 57, pp. 268–435.

[2] R. Irving, N. A. Scarlett: Wear 1964, vol. 7, pp. 244–254.

[3] Y. Matsubara, H. Hamada: A novel method to evaluate the influence of hydrogen on fatigue properties of high strength steels: in: J. M. Beswick (Ed.), Bearing Steel Technology - Advances and State of the Art in Bearing Steel Quality Assurance: ASTM International, West Conshohocken, PA, USA, 2007: pp. 153–166.

[4] M.-H. Evans: Materials Science and Technology 2012, vol. 28, pp. 3–22.

[5] P. Schatzberg, I. M. Felsen: Wear 1968, vol. 12, pp. 331–342.

[6] K. Tamada, H. Tanaka: Wear 1996, vol. 199, pp. 245–252.

[7] L. Grunberg, D. T. Jamieson, D. Scott: Philosophical Magazine 1963, vol. 8, pp. 1553–1568.

[8] T. Imran, B. Jacobson, A. Shariff: Wear 2006, vol. 261, pp. 86–95.

[9] R. A. Oriani: Corrosion 1987, vol. 43, pp. 390–397.

[10] H. K. Brinbaum, P. Sofronis: Materials Science & Engineering A 1994, vol. 176, pp. 191–202.

[11] A. R. Troiano: Trans. ASM 1960, vol. 52, pp. 54–80.

[12] E. J. Song, H. K. D. H. Bhadeshia, D.-W. Suh: Corrosion Science 2013, vol. 77, pp. 379–384.

[13] M. Śmiałowski: Hydrogen in steel; effect of hydrogen on iron and steel during production, fabrication and use: Pergamon Press, Oxford, U. K., 1962.

[14] G. M. Pressouyre: Metallurgical and Materials Transactions A 1979, vol. 10, pp. 1571–1573.

[15] J. P. Hirth: Metallurgical & Materials Transactions A 1980, vol. 11 (861–890).

[16] W. Solano-Alvarez, H. K. D. H. Bhadeshia: Metallurgical and Materials Transactions A 2014, vol. 45 (11), pp. 4907–4915.

[17] W. Solano-Alvarez, H. K. D. H. Bhadeshia: Metallurgical and Materials Transactions A 2014, vol. 45 (11), pp. 4916–4931.

[18] C. A. Stickels: Metallurgical Transactions 1974, vol. 5, pp. 865–874.

[19] B. D. Craig: Acta Metallurgica 1977, vol. 25, pp. 1027–1030.

[20] A. T. W. Barrow, J. H. Kang, P. E. J. R.-D. del Castillo: Acta Materialia 2012, vol. 60 (6), pp. 2805–2815.

[21] K. Kawakami, T. Matsumiya: ISIJ international 2013, vol. 53 (4), pp. 709–713.

[22] M. A. V. Devanathan, Z. Stachurski: Proceedings of the Royal Society of London. Series A. Mathematical and Physical Sciences 1962, vol. 270 (1340), pp. 90–102.

[23] ISO-17081: Method of measurement of hydrogen permeation and determination of hydrogen uptake and transport in metals by an electrochemical technique: Tech. rep. 2004,.

[24] D. K. Han, K. Y. Kim, S. J. Kim, H. G. Jung: Effect of heat treatment on hydrogen diffusion and hydrogen induced cracking behavior of process pipe steel in sour environment: in: The Twenty-third International Offshore and Polar Engineering Conference: International Society of Offshore and Polar Engineers, 2013.

[25] T. Tarui, M. Kubota: Approaches for fundamental principles 1: Evaluation method of hydrogen embrittlement and improvement techniques of delayed fracture: Tech. Rep. 101: Nippon Steel 2012,.

[26] L. C. D. Fielding, E. J. Song, D. K. Han, H. K. D. H. Bhadeshia, D.-W. Suh: Proceedings of the Royal Society A 2014, vol. 470 (20140108).

[27] E. J. Song, D. W. Suh, H. K. D. H. Bhadeshia: Computational Materials Science 2013, vol. 79, pp. 36–44.

[28] H. Swahn, P. C. Becker, O. Vingsbo: Metal Science 1976, vol. 10, pp. 35–39.

[29] O. D. Gonzalez: Transactions of the Metalurgical Society, American Instiute of Mining, Metalurgical and Petroleum Enginers 1969, vol. 245 (607-612).

[30] J. W. Christian: Thermodynamics and kinetics of martensite: in: G. B. Olson, M. Cohen (Eds.), International Conference on Martensitic Transformations ICOMAT '79: Alpine Press, Massachusetts, USA, 1979: pp. 220–234.

[31] K. Huber, G. Herzberg: Molecular Spectra and Molecular Structure 4: Constants of Diatomic Molecules: Van Norstrand Reinhold Co, New York, 1979.

[32] R. Gibala, J. Ratka, J. Talia, S. Wu: Environmental reactions and their effects on mechanical behavior of metallic materials: Technical progress report: Case Western Reserve University 1980,.